Langmuir

Article

pubs.acs.org/Langmuir

Spontaneous Aggregate Transition in Mixtures of a Cationic Gemini Surfactant with a Double-Chain Cationic Surfactant

Maozhang Tian,[†] Yaxun Fan,[†] Gang Ji,[‡] and Yilin Wang*[,†]

[†]Key Laboratory of Colloid and Interface Science, Beijing National Laboratory for Molecular Sciences (BNLMS), Institute of Chemistry, Chinese Academy of Sciences, Beijing 100190, People's Republic of China

[‡]Center for Biological Electron Microscopy, Institute of Biophysics, Chinese Academy of Sciences, Beijing 100101, People's Republic of China

Supporting Information

ABSTRACT: Controllable aggregate transitions were realized by mixing two kinds of cationic surfactants, hexylene-1,6-bis(dodecyldimethylammonium bromide) ($C_{12}C_6C_{12}Br_2$) and didodecyldimethylammonium bromide (DDAB). It was found that two parameters are the main factors determining the aggregation behavior of the mixed system, the total concentration of DDAB and $C_{12}C_6C_{12}Br_2$ (C_T), and the mole fraction of DDAB in the mixtures of DDAB and $C_{12}C_6C_{12}Br_2$ (X_{DDAB}). How these two parameters act on the aggregate transitions was studied in detail by various measurements including surface tension, turbidity, electrical conductivity, ζ potential, isothermal titration microcalorimetry, dynamic light scattering, cryogenic transmission electron microscopy, and ^{1}H NMR. When C_T was constant, spontaneous vesicle-to-micelle transitions were found with decreasing X_{DDAB} at high C_T. When X_{DDAB} was constant, aggregate transitions were generated by gradually increasing C_T, depending on different X_{DDAB} ranges. At $X_{DDAB} < 0.6$, small spherical aggregates formed first and then transferred to vesicles, and finally the vesicles transitioned to micelles. At $X_{DDAB} \geq 0.6$, the progressive increase in C_T led to aggregate transitions on the order of the arising of vesicles, the continuous growth of vesicles, the disruption of vesicles into micelles, and the final coexistence of vesicles and micelles. The hydrophobic interaction and electrostatic repulsion between DDAB and $C_{12}C_6C_{12}Br_2$ together with the related degree of ionization and hydration of the surfactants were gradually adjusted by changing the ratio and the total concentration of these two surfactants, which should be responsible for the complicated aggregation behavior.

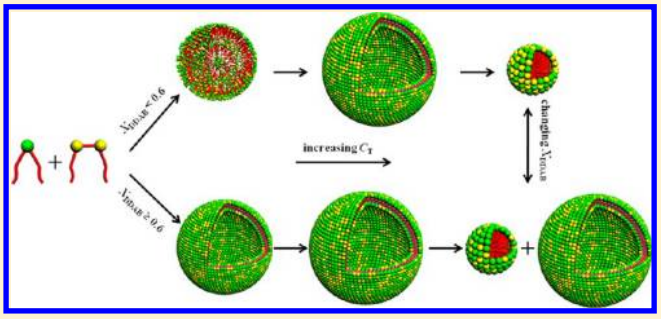

INTRODUCTION

Self-assemblies of surfactants such as vesicles and micelles have attracted much attention from an elementary perspective as well as for their widespread applications.[1−3] In particular, transitions between vesicles and micelles are of great interest because of their potential applications in drug encapsulation and release, gene delivery, and so forth. Usually, the aggregation behaviors of surfactants are controlled by electrostatic, van der Waals, hydrophobic, and steric interactions as well as their delicate balance.[4] Although great endeavors have been devoted to explicate these weak interactions in manipulating the self-assembly processes, further comprehension is still in need of more systematic research.

Until now, to realize the transition between vesicles and micelles, various methods have been introduced, among which mixing different surfactants have been proved to be one of the effective methods.[5−13] Lichtenberg[14] brought forward that the effect of the mixed ratio stood out as the mainstay in the aggregate transitions through adding micelle solutions into vesicular solutions. By changing the mixed ratios, aggregates with varied structures and sizes were obtained.[15−20] Edwards' group[17] studied the vesicle-to-micelle transition process in mixed solutions of dodecyl octaethylene glycol monoether ($C_{12}E_8$) and lecithin. Vesicle growth was observed while initially adding $C_{12}E_8$ to the lecithin solution because of the fusion of the vesicular membranes. Then the progressive enhancement of the $C_{12}E_8$ concentration led to vesicle saturation by $C_{12}E_8$ and formed threadlike micelles. Finally, the mixed threadlike micelles were transformed into globular micelles. In this case, an effective packing parameter[21] was introduced to explain the formation of the threadlike micelles. The solubilization of lecithin vesicles by alkyl sulfate surfactants ($C_{10}SO_4^-$, $C_{12}SO_4^-$, and $C_{14}SO_4^-$) was also investigated.[20] It indicated that the added $C_{10}SO_4^-$ led to lamellar aggregates and threadlike micelles whereas the addition of $C_{12}SO_4^-$ and $C_{14}SO_4^-$ gave rise to a holey lamellar phase. In a word, either the mixed ratio or the surfactant structures have a profound influence on the morphology of the mixed aggregates.

Gemini surfactants[22−24] are superior to the corresponding conventional single-chain surfactants because of their special

Received: April 30, 2012
Revised: June 29, 2012
Published: July 24, 2012

self-assembling ability. Zana's group[25] synthesized a series of alkanediyl-α,ω-(dimethylalky1ammonium bromide) surfactants, referred to as $C_mC_sC_mBr_2$ surfactants (m and s stand for the number of carbons in the alkyl chains and spacer, respectively). The aggregate transition between vesicles and micelles was investigated by introducing gemini surfactants with different spacer lengths. It was found that adding micelle solutions of both dodecyltrimethylammonium bromide DTAB and $C_{12}C_{10}C_{12}Br_2$ to the vesicular solutions of $C_{12}C_{20}C_{12}Br_2$ brought about the transition from vesicles to micelles, but intermediate aggregates displayed different structures.[26] The initial addition of DTAB to the $C_{12}C_{20}C_{12}Br_2$ solution led to small vesicles whereas the addition of $C_{12}C_{10}C_{12}Br_2$ brought about vesicle growth. When a threadlike micelle solution of $C_{12}C_2C_{12}Br_2$ was mixed with the $C_{12}C_{20}C_{12}Br_2$ vesicles,[27] vesicle growth was observed at a low $C_{12}C_2C_{12}Br_2$ molar ratio. Nevertheless, with further increases in the $C_{12}C_2C_{12}Br_2$ molar ratio, disklike, ringlike, and threadlike micelles appeared and finally network aggregates formed by the interconnected threads and rings. These elaborated works showed that a gradual variation in aggregate structures might be achieved by the variations of electrostatic repulsion and hydrophobic force.

Cationic ammonium gemini surfactant $C_{12}C_6C_{12}Br_2$ has an intermediate spacer length and can self-assemble into spherical micelles in aqueous solution. Didodecyldimethylammonium bromide, DDAB, is a double-chained cationic surfactant and normally forms vesicles in aqueous solution.[28−30] Because both DDAB and $C_{12}C_6C_{12}Br_2$ are quaternary ammonium salts and have two alkyl chains of equal length, the only difference exists in their headgroups. Mixing DDAB and $C_{12}C_6C_{12}Br_2$ may gradually change the average area of their headgroups and finely adjust the DDAB/$C_{12}C_6C_{12}Br_2$ mixed aggregates in aqueous solution through varying the mixed ratio and total concentration. In the present work, surface tension, turbidity, conductivity, isothermal titration microcalorimetry (ITC), dynamic light scattering (DLS), zeta potentials, ^{1}H NMR, and cryogenic transmission electron microscopy (cryo-TEM) have been employed to characterize the aggregate transitions in the mixed DDAB/$C_{12}C_6C_{12}Br_2$ aqueous solution, and the related interaction mechanism has been discussed. The results may help us to understand the molecular interaction in the bicationic mixed surfactants and provide guidance to adjust weak interactions elaborately in the mixed surfactants and in turn construct surfactant aggregates with different properties.

EXPERIMENTAL SECTION

Materials. Cationic gemini surfactant $C_{12}C_6C_{12}Br_2$ was synthesized and purified according to the literature.[31] Cationic surfactant DDAB was purchased from the TCI Company with a purity higher than 99%. The water used to preparing the mixture solution in all experiments was from Milli-Q. The resistivity of the Milli-Q water is 18.2 MΩ.cm.

Surface Tension Measurements. The surface tension of the mixed system in different mixed ratios was measured using the drop volume method.[32] Each drop was kept for about 20 min or half an hour, and the value of γ was determined from at least five consistent measured values. Each surface tension curve was repeated at least two times. The measurement temperature was controlled at 25.00 ± 0.05 °C using a thermostat.

Turbidity Measurements. The turbidity of the mixed system at different X_{DDAB} values was measured at 450 nm using a Brinkmann PC920 probe colorimeter. The turbidity is expressed on a relative scale. Before the measurements were carried out, the probe was put into triply distilled water whose turbidity was set to zero. Then the mixtures of DDAB/$C_{12}C_6C_{12}Br_2$ were titrated into water gradually, and the turbidity of the mixed solution was obtained. The final turbidity value was recorded after the value became stable (after at least 5 min). The measurement was performed in a double-walled glass container with water circulation, and the temperature was controlled at 25.0 ± 0.1 °C by a water-circulating thermostat.

Electrical Conductivity Measurements. The conductivity of the mixed system at different X_{DDAB} values was measured as a function of concentration using a JENWAY model 4320 conductivity meter. A mixed solution of DDAB and $C_{12}C_6C_{12}Br_2$ was titrated into water gradually, and the conductivity value was recorded after the value became stable. The measurement was performed in a double-walled glass container with the circulation of water, and the temperature was controlled at 25.0 ± 0.1 °C by a water-circulating thermostat.

Isothermal Titration Microcalorimetry (ITC). A TAM 2277-201 isothermal titration microcalorimeter (Thermometric AB, Sweden) was used to measure the enthalpy change of the aggregate transitions in the mixed solution. The sample cell and the reference cell of the microcalorimeter were initially loaded with 700 and 815 μL of pure water, respectively. A mixed solution with different concentrations was injected consecutively into the stirred sample cell in portions of 10 μL using a 500 μL Hamilton syringe controlled by a Thermometric 612 Lund pump until the desired concentration range had been covered. During the whole titration process, the system was stirred at 60 rpm with a gold propeller, and the interval between two injections was long enough for the signal to return to the baseline. The observed enthalpy (ΔH_{obs}) was obtained by integrating the areas of the peaks in the plot of thermal power against time. The reproducibility of the experiments was within ±4%. All measurements were performed at 25.00 ± 0.01 °C.

Dynamic Light Scattering (DLS). Measurements were carried out with an LLS spectrometer (ALV/SP-125) with a multi-τ digital time correlator (ALV-5000). A solid-state He−Ne laser (output power of 22 mW at λ = 632.8 nm) was used as a light source, and the measurements were conducted at a scattering angle of 90°. The freshly prepared samples were injected into a 7 mL glass bottle through a 0.45 μm filter prior to measurements. The correlation function of the scattering data was analyzed via the CONTIN method to obtain the distribution of diffusion coefficients (D) of the solutes, and then the apparent equivalent hydrodynamic radius (R_h) was determined using the Stokes−Einstein equation $R_h = kT/6\pi\eta D$, where k is the Boltzmann constant, T is the absolute temperature, and η is the solvent viscosity. All measurements were performed at 25.00 ± 0.01 °C.

ζ-Potential Measurements. ζ potential characterization of the surface charge of the aggregates in the mixed solution was carried out at 25 °C and at a scattering angle of 173° with a ZetaSizer Nano Series Nano ZS (Malvern Instruments) equipped with a thermostatted chamber and employing a 4 mW He−Ne laser (λ = 632.8 nm). The ζ potential was investigated using 600 μL of sample solution in a standard cuvette provided by Malvern.

Cryogenic Transmission Electron Microscopy (Cryo-TEM). The samples were embedded in a thin layer of vitreous ice on freshly carbon-coated holey TEM grids by blotting the grids with filter paper and then plunging them into liquid ethane cooled by liquid nitrogen. Frozen hydrated specimens were imaged by using an FEI Tecnai 20 electron microscope (LaB6) operated at 200 kV in low-dose mode (about 2000 e/nm^2) and a nominal magnification of 50 000. For each specimen area, the defocus was set to 1 to 2 μm. Images were recorded on Kodak SO 163 films and then digitized by a Nikon 9000 with a scanning step of 2000 dpi corresponding to 2.54 Å/pixel.

^{1}H NMR. ^{1}H NMR spectra were recorded using a Bruker AV400 FT-NMR spectrometer operating at 400.1 MHz at room temperature (25 ± 2 °C). Deuterium oxide (99.9%) was purchased from CIL (Cambridge Isotope Laboratories) and used to prepare the stock solutions of the surfactants. About 1 mL of solution was transferred to a 5 mm NMR tube for each measurement. Chemical shifts were given on the parts per million scale. The center of the HDO signal (4.790 ppm) was used as the reference in the D_2O solutions. The digital resolution of the ^{1}H NMR spectra was 0.04 Hz/data point.

dx.doi.org/10.1021/la301762g | Langmuir 2012, 28, 12005−12014

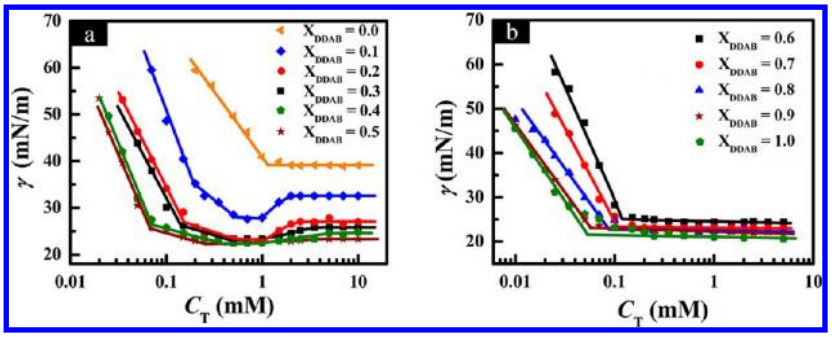

Figure 1. Surface tension of the mixed DDAB/$C_{12}C_6C_{12}Br_2$ solutions plotted against C_T at different X_{DDAB} values at 25.0 °C.

RESULTS AND DISCUSSION

In this section, in order to display the variation situation of the mixed DDAB/$C_{12}C_6C_{12}Br_2$ system completely, the experimental results at different mixing molar fractions (X_{DDAB}) and as a function of the total surfactant concentration (C_T) will be introduced first. Because the results indicate that the self-assembly behaviors are distinguished at $X_{DDAB} < 0.6$ from those at $X_{DDAB} \geq 0.6$, the situations at $X_{DDAB} = 0.3$ and 0.8 will be chosen as representatives to discuss the aggregate transitions in detail.

Surface Tension. Surface tension measurements on the mixed DDAB/$C_{12}C_6C_{12}Br_2$ solutions were carried out as a function of the total surfactant concentration (C_T) at different molar fractions of DDAB (X_{DDAB}) from 0.0 to 1.0. The curves are classified into two groups (Figure 1a,b) according to their features.

Figure 1a shows the surface tension curves at $0 \leq X_{DDAB} < 0.6$. In detail, for $X_{DDAB} = 0.0$ (pure $C_{12}C_6C_{12}Br_2$ solution), the curve shows a critical concentration at 1.02 mM, which is the critical micelle concentration of $C_{12}C_6C_{12}Br_2$ and is in good agreement with the literature.[31] For $0 < X_{DDAB} < 0.6$, all of the curves have three inflection points. In the lower-concentration region, the surface tension decreases rapidly to the first inflection point with increasing C_T and then gradually goes down to the second inflection point, followed by a short period of the lowest constant surface tension. When C_T is beyond ~1.0 mM, the surface tension increases above the third inflection point and finally levels off. This unique changing trend of the curves presents a special "basin" shape, which was rarely found in other bicationic surfactant systems. Moreover, it can be found that the increase in X_{DDAB} not only gradually reduces the critical surfactant concentration at the first inflection point but also significantly reduces the surface tension.

Figure 1b presents the surface tension curves in the region of $0.6 \leq X_{DDAB} < 1.0$. In contrast to Figure 1a, there is only one critical concentration for each curve, just like normal surface tension curves of surfactants. Besides, both the critical concentration and the surface tension decrease only slightly as X_{DDAB} increases.

The surface tension curves reflect the variation in the surfactant molecular arrangement at the air/water interface. These surface tension curves imply that the DDAB/$C_{12}C_6C_{12}Br_2$ mixtures may have three kinds of molecular packing modes at the air/water interface at X_{DDAB} lower than 0.6 and may have only one at X_{DDAB} equal to or larger than 0.6. To understand the aggregation behavior in the bulk solution, more techniques were employed as follows.

Turbidity. The turbidity measurement is a convenient method of characterizing the aggregate transition in solution from a macroscopic viewpoint. It cannot determine the values of aggregate size, but it can reflect the decreasing or increasing tendency of the aggregates. Although DLS is a normal method of determining the size distribution of the aggregates in solution, it cannot determine the relative contents of different aggregates because large aggregates have strong scattering intensities. Even using the number-weighted method, DLS often gives out unbelievable results about the relative contents of aggregates. Especially for ionic gemini surfactants, DLS often cannot present the real size for the highly charged aggregates because the diffusion coefficients measured by DLS are strongly influenced by electrostatic repulsion among highly charged aggregates. Therefore, the turbidity measurement is a necessary approach to revealing the real situation about the variation tendency of aggregate size, from which it can be confirmed if the aggregate transitions take place and the critical points of the transitions can be determined. Herein, the turbidity is plotted against C_T at different X_{DDAB} values given in Figure 2. For

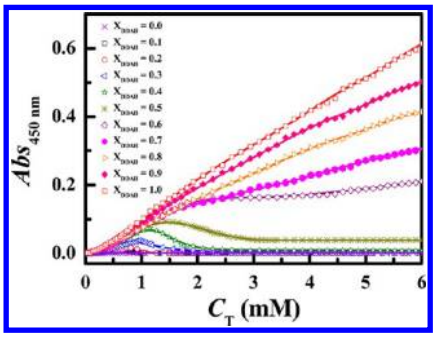

Figure 2. Turbidity of the mixed DDAB/$C_{12}C_6C_{12}Br_2$ solutions plotted against C_T at different X_{DDAB} values at 25.0 °C.

$X_{DDAB} = 0.0$, the turbidity is close to that of water over the whole concentration range. Normally, the turbidity of dilute small micelle solutions is very close to that of water (i.e., is very close to zero). The turbidity by the colorimeter used here can reflect more significant variations in the aggregate size. For $0.1 \leq X_{DDAB} < 0.6$, with the increase in C_T, the turbidity increases gradually to a maximum and then decreases until attaining a low constant value. Moreover, with the increase in X_{DDAB}, the turbidity peak is weakened gradually. Until X_{DDAB} reaches 0.6, the turbidity versus C_T curve becomes a platform instead of the peak after the initial increasing stage. When $X_{DDAB} > 0.6$, the turbidity curves keep rising with increasing C_T over the whole C_T region, but the rising rate is slightly lower in the high-C_T region compared to that in the low-C_T region. These results indicate that when $X_{DDAB} \geq 0.6$ the mixed aggregates in the solution may become larger gradually with the increase in the

dx.doi.org/10.1021/la301762g | Langmuir 2012, 28, 12005−12014

total surfactant concentration, whereas for $X_{DDAB} < 0.6$, the aggregate size experiences an increasing and then a decreasing process.

Electrical Conductivity. To know the ionization situation of the mixed DDAB/$C_{12}C_6C_{12}Br_2$ aggregates, the conductivity was measured as a function of C_T at different X_{DDAB} values, as shown in Figure 3. It should be pointed out that there are two

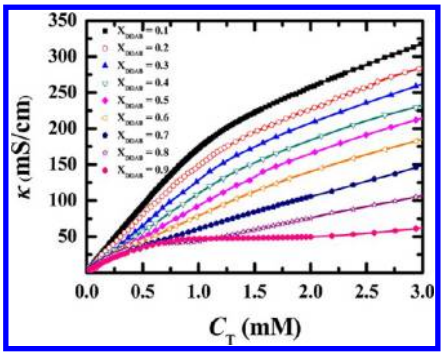

Figure 3. Electrical conductivity (κ) of the mixed DDAB/$C_{12}C_6C_{12}Br_2$ solutions plotted against C_T at different X_{DDAB} values at 25.0 °C.

critical concentrations at $0.1 \leq X_{DDAB} \leq 0.6$ and three critical concentrations at $0.6 < X_{DDAB} \leq 0.9$. The critical points can be seen more clearly in Figure S1 of the Supporting Information presented as individual curves, which also presents the determinations of the critical concentrations from the conductivity curves. At $0.1 \leq X_{DDAB} < 0.6$, the electrical conductivity curves keep increasing with increasing C_T over the whole C_T range, but the rate of increase is smaller above these two critical concentrations. As for $0.8 \leq X_{DDAB} \leq 0.9$, the conductivity increases with a smaller rate of increase above the first critical concentration, remains nearly unchanged between the second and third critical concentrations, and then begins to increase above the third critical concentration. At $0.6 \leq X_{DDAB} \leq 0.7$, there are also three critical concentrations, but the conductivity is still increasing between the second and third critical concentrations. In brief, these results suggest when X_{DDAB} is smaller than 0.6 two aggregate transitions are detected with increasing C_T and the aggregation degree of ionization of the mixed aggregates decreases with the transitions. Although X_{DDAB} is equal to or larger than 0.6, the aggregation degree of ionization experiences a decreasing and then an increasing process with increasing C_T.

ITC. Microcalorimetry is a powerful tool for investigating physical and chemical processes accompanied by the release or uptake of heat. In particular, ITC has an advantages in characterizing aggregate transitions and understanding the intermolecular interactions in the transitions.[33] Here, ITC measurements were carried out to measure the observed enthalpy ΔH_{obs} with the titration of the mixed solutions of DDAB and $C_{12}C_6C_{12}Br_2$ (initial C_T is 10.0 mM) in water at different X_{DDAB} values. Figure 4 shows the curves of the observed enthalpy ΔH_{obs} against the final surfactant concentration. All of the variations in the ITC curves follow regular patterns, depending on the mixed ratio. The ITC curve at $X_{DDAB} = 0$ reflects the micellization process of $C_{12}C_6C_{12}Br_2$ itself. Similar to many ionic surfactants, this ITC curve is approximately sigmoidal in shape and can be subdivided into two concentration regions separated by a transition region, corresponding to the cmc of $C_{12}C_6C_{12}Br_2$. When C is below cmc, all added micelles are demicellized into monomers and the

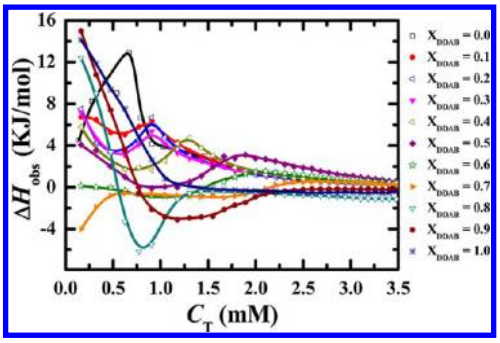

Figure 4. Observed enthalpy ΔH_{obs} of the mixed DDAB/$C_{12}C_6C_{12}Br_2$ solutions of 10.0 mM at different X_{DDAB} values being titrated into water vs the final C_T at 25.00 °C.

monomers are further diluted. When C is greater than the cmc, only the micellar solution is diluted and finally drops toward zero. The titration process is actually the demicellization process. Although the observed enthalpy ΔH_{obs} is endothermic, the micellization enthalpy determined from the enthalpy difference between the two segments of the enthalpy curves extrapolated to the cmc is exothermic. At $0.1 \leq X_{DDAB} \leq 0.6$, upon titrating the mixtures of DDAB and $C_{12}C_6C_{12}Br_2$ into water, the ΔH_{obs} values are all endothermic, but the values follow decreasing, increasing, and then decreasing modes. Thus, the ITC curves display a minimum and then a maximum, which all move to larger surfactant concentrations with the increase in X_{DDAB}. At $0.7 < X_{DDAB} \leq 0.9$, with the titrations of the mixtures of DDAB and $C_{12}C_6C_{12}Br_2$ into water, ΔH_{obs} changes from a larger endothermic value to an exothermic value and then tends to zero. For the case at $X_{DDAB} = 0.7$, the initial endothermic enthalpy does not appear, possibly because the surfactant concentration is not low enough. In general, the manifold energy alteration indicates the variation in the molecular interactions in the aggregate transition processes.

In total, the critical concentrations obtained by surface tension, conductivity, turbidity, and ΔH_{obs} measurements are consistent. The critical concentrations in the surface tension curves can be attributed to the variation in the molecular arrangement at the air/water interface, whereas other curves reflect the aggregation behaviors in the bulk solution. The coincidence of the critical points suggests that the assembling transitions occur at the interface and in the bulk solution simultaneously.

On the basis of all of the above results, obviously the self-assembly behavior of the DDAB/$C_{12}C_6C_{12}Br_2$ mixture is greatly dependent on X_{DDAB}. The variation in the self-assembly behaviors is distinguished at $X_{DDAB} < 0.6$ from that at $X_{DDAB} \geq 0.6$. Thus, to gain deeper insight into the aggregation behaviors of the mixed system, the situations at $X_{DDAB} = 0.3$ and 0.8 are chosen as representatives for discussing the aggregate transition processes in detail. In addition, the ζ potential, DLS intensity, cryo-TEM, and ^{1}H spectra of the mixed DDAB/$C_{12}C_6C_{12}Br_2$ solutions were carried out for these two representative mixing ratios.

Aggregation Behavior at $X_{DDAB} = 0.3$. Figure 5 summarizes the (a) surface tension, (b) turbidity, (c) electrical conductivity, (d) observed enthalpy change, (e) ζ potential, and (f) DLS intensity of the mixed DDAB/$C_{12}C_6C_{12}Br_2$ solutions plotted against C_T at $X_{DDAB} = 0.3$. Also, to understand the energy change in the aggregate transitions better, the observed enthalpy change ΔH_{obs} was studied against C_T via

dx.doi.org/10.1021/la301762g | Langmuir 2012, 28, 12005−12014

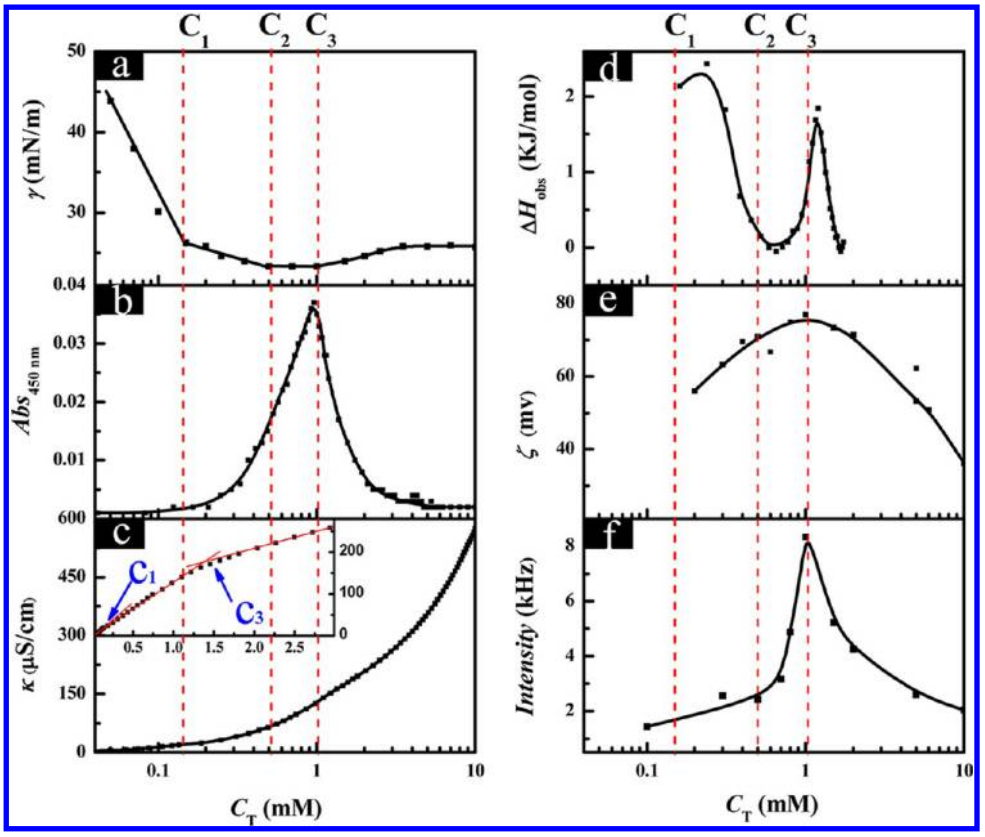

Figure 5. Variations of the (a) surface tension, (b) turbidity, (c) electrical conductivity, (d) observed enthalpy change, (e) ζ potential, and (f) DLS intensity of the DDAB and $C_{12}C_6C_{12}Br_2$ mixtures plotted against C_T on a logarithmic scale at 25.0 °C (X_{DDAB} = 0.3).

titrating the DDAB/$C_{12}C_6C_{12}Br_2$ mixtures with different initial total concentrations (i.e., 10.0, 5.0, and 2.0 mM) into water (Figure 6). By combining all of the curves from different techniques, obviously the curves against C_T can be divided into four regions, which are below C_1 (C_T < 0.16 mM), between C_1 and C_2 (0.16−0.51 mM), between C_2 and C_3 (0.51−1.02 mM), and beyond C_3 (C_T > 1.02 mM). The morphologies of the mixed DDAB/$C_{12}C_6C_{12}Br_2$ aggregates in the four regions were characterized by cryo-TEM. Below C_1, no aggregates were formed. Figure 7 shows representative images of the aggregates at C_T = 0.3, 0.9, and 10.0 mM, which were selected from the concentration regions of C_1 to C_2, C_2 to C_3, and beyond C_3, respectively. Repeated observations were carried out, and some images are included in the Supporting Information.

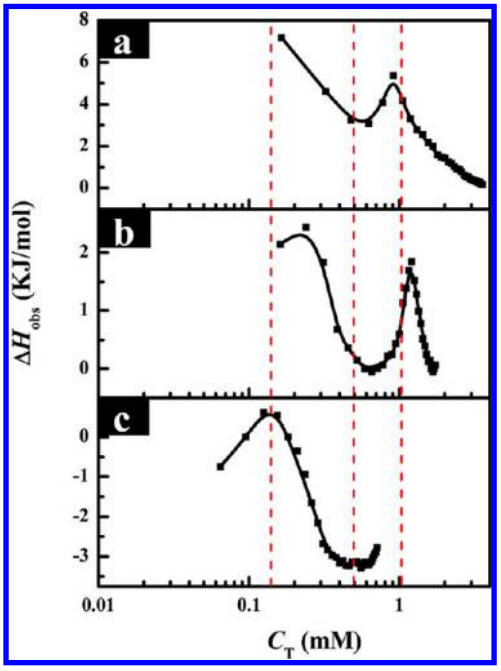

Figure 6. Observed enthalpy ΔH_{obs} vs C_T on a logarithmic scale for the titration of the DDAB/$C_{12}C_6C_{12}Br_2$ mixed solution with initial concentrations of (a) 10.00 mM, (b) 5.00 mM, and (c) 2.00 mM into water at 25.00 °C (X_{DDAB} = 0.3).

As shown in Figures 5 and 6, all of the curves present a critical point at C_1 except the ζ potential and light scattering intensity curves. Correspondingly, below C_1, no aggregates were observed by cryo-TEM. Beyond C_1, the turbidity, ζ potential, and light scattering intensity increase gradually as C_T increases. Meanwhile, the slope of the conductivity curve decreases, reflecting a decreased aggregation degree of ionization, accompanied by a decreasing endothermic ΔH_{obs} in the ITC curve. The cryo-TEM image (Figure 7a) shows spherical aggregates of ~20 nm diameter in the region of C_1 to C_2. These spherical aggregates are evidently larger than the traditional spherical micelles, and the same phenomena were also obtained by other researchers, which were speculated to be "embryo-like vesicles with an interdigitated bilayer fragment".[34] All of these results indicate that the mixed surfactants start to aggregate and form spherical aggregates beyond C_1.

In the region of C_2 to C_3, unilamellar vesicles with smooth curved bilayers (Figure 7b), smaller vesicles inside larger ones (Figure 7c), and double multilamellar vesicles (Figure S2) are clearly seen in the cryo-TEM images, indicating that vesicles are

dx.doi.org/10.1021/la301762g | Langmuir 2012, 28, 12005−12014

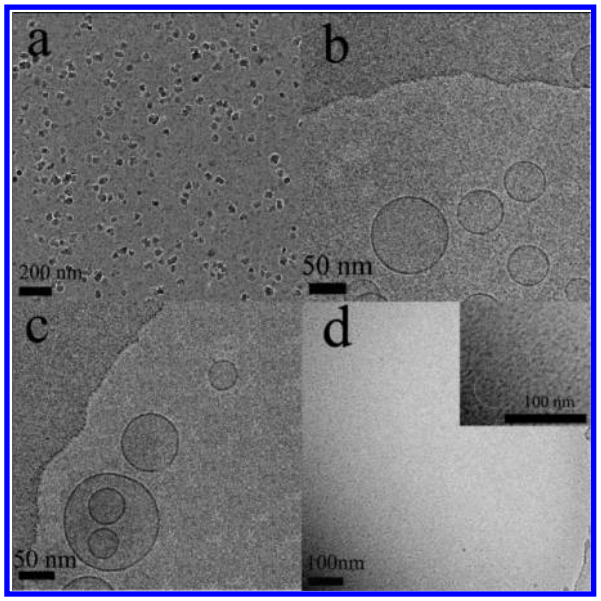

Figure 7. Cryo-TEM micrographs of the DDAB/$C_{12}C_6C_{12}Br_2$ aggregates (X_{DDAB} = 0.3) at C_T values of (a) 0.3, (b, c) 0.9, and (d) 10.0 mM. The inset of d is an enlarged image of small spherical micelles.

the dominant aggregates in this region. Correspondingly, in Figure 5, it can be seen that the turbidity, conductivity, ζ potential, and the light scattering intensity increase promptly beyond C_2, and the observed enthalpy changes from approximately zero to endothermic. Meanwhile, the surface tension reaches a considerably low value at C_2, close to the value of the pure DDAB solution, and stays constant afterward. Thus, it can be assumed that the lower surface tension may mainly result from the arrangement of DDAB molecules at the air/solution interface. These results demonstrate that beyond C_2 the spherical aggregates transfer to spherical vesicles that display a higher surface charge density than the spherical aggregates.

Beyond C_3, the cryo-TEM images (Figure 7d) show that the mixed aggregates are spherical micelles of ~2 nm, demonstrating that the vesicles start to transfer to small micelles. Meanwhile, the turbidity, ζ potential, and light scattering intensity in Figure 6 decrease significantly after C_3 whereas the surface tension gets larger. The above information shows that the large vesicles transfer to small spherical micelles in this region.

Generally, the transformation from vesicles to micelles should be an endothermic process induced by the synergistic effect of hydrophobic interactions and electrostatic interactions of surfactants. Moreover, at a given surfactant concentration, a large number of small aggregates should have a higher degree of ionization than a small number of larger aggregates.[35,36] However, in this bicationic system, the endothermic ΔH_{obs} value decreases gradually and the conductivity curve reflects a decreased degree of aggregation ionization in the vesicle-to-micelle transition. To obtain a feasible explanation, more investigations were carried out as follows.

A systematic ITC study was performed by titrating the DDAB/$C_{12}C_6C_{12}Br_2$ mixed solution with different initial concentrations into water (Figure 6). All of the initial concentrations are higher than C_3. That is to say that the DDAB/$C_{12}C_6C_{12}Br_2$ mixtures exist as micelles in the initial solutions of 10.0 and 5.0 mM (far beyond C_3) but exist as the micelle/vesicle mixture in the initial solution of 2.0 mM (just above C_3). When the final C_T is located at C_1 to C_2 and C_2 to C_3 (Figure 6a,b), all of the ΔH_{obs} values are endothermic, indicating that both the micelle-to-spherical aggregate transition and the micelle-to-vesicle transition are endothermic processes. As for the ITC titration of the DDAB/$C_{12}C_6C_{12}Br_2$ vesicles and the micelle solution into water (Figure 6c), when the final concentration C_T is below C_1, the ΔH_{obs} value is exothermic, which indicates that the process of the micelles and vesicles breaking up into surfactant monomers must be accompanied by the strong hydration and ionization of the surfactants, whereas the final concentration C_T is located between C_1 and C_2, the steeply increasing, exothermic ΔH_{obs} suggests that the transition of the vesicles/micelles into spherical aggregates is exothermic. Considering that the degree of ionization of the surfactants decreases in the order of spherical aggregates, vesicles, and micelles and that the increase in the degree of ionization can strengthen the electrostatic repulsion between the headgroups, the headgroup packing becomes more compact in the order of spherical aggregates, vesicles, and micelles. Meanwhile, in the transitions from spherical aggregates to vesicles and micelles, the surfactant concentration increases. On the basis of the possible structures of these aggregates, the hydrophobic interaction between the hydrophobic chains in the vesicles should be weaker than in the micelles but stronger than in the spherical aggregates. All of these variations in the degree of ionization and hydrophobic interaction accompanying the variation in hydration determine the above enthalpy change in the aggregate transitions.

Normally, aggregate transitions have a significant influence on the chemical environment of protons and thus bring about a gradual change in the chemical shifts ($\Delta\delta$).[35,36] Therefore, analyzing the relationship between $\Delta\delta$ of the proton signals and surfactant concentration has become an effective way to investigate the aggregation behaviors. ^{1}H NMR spectra and proton assignments of the mixed surfactants versus different C_T values at X_{DDAB} = 0.3 are shown in Figure 8. Calculated $\Delta\delta$

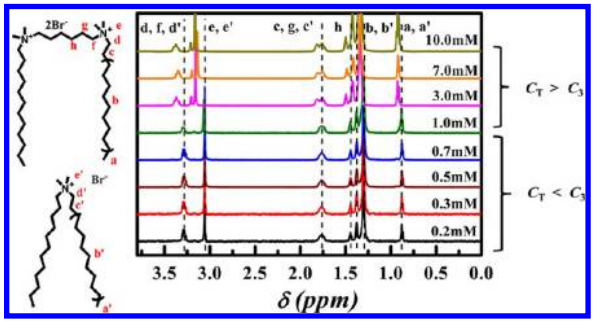

Figure 8. ^{1}H NMR spectra and proton assignments of the DDAB/$C_{12}C_6C_{12}Br_2$ mixtures at different C_T values in D_2O at X_{DDAB} = 0.3.

plotted against C_T is shown in Figure S4. It can be observed that the chemical shifts of the protons remain constant below C_3, which indicates that the environment of the protons in the transition from spherical aggregates to vesicles has no obvious changes. Another possible reason is that the aggregates are large, as a result of which the effect of the aggregation on the signals of the protons may be weaker. However, the protons move to low field above C_3. The protons in the tail groups (H_a, $H_{a'}$, H_b, $H_{b'}$, H_c, and $H_{c'}$) and the spacer groups (H_h and H_g) shift to low field slightly, whereas the protons in the headgroups (H_d, $H_{d'}$, H_e, $H_{e'}$, and H_f) shift to low field greatly.

dx.doi.org/10.1021/la301762g | Langmuir 2012, 28, 12005−12014

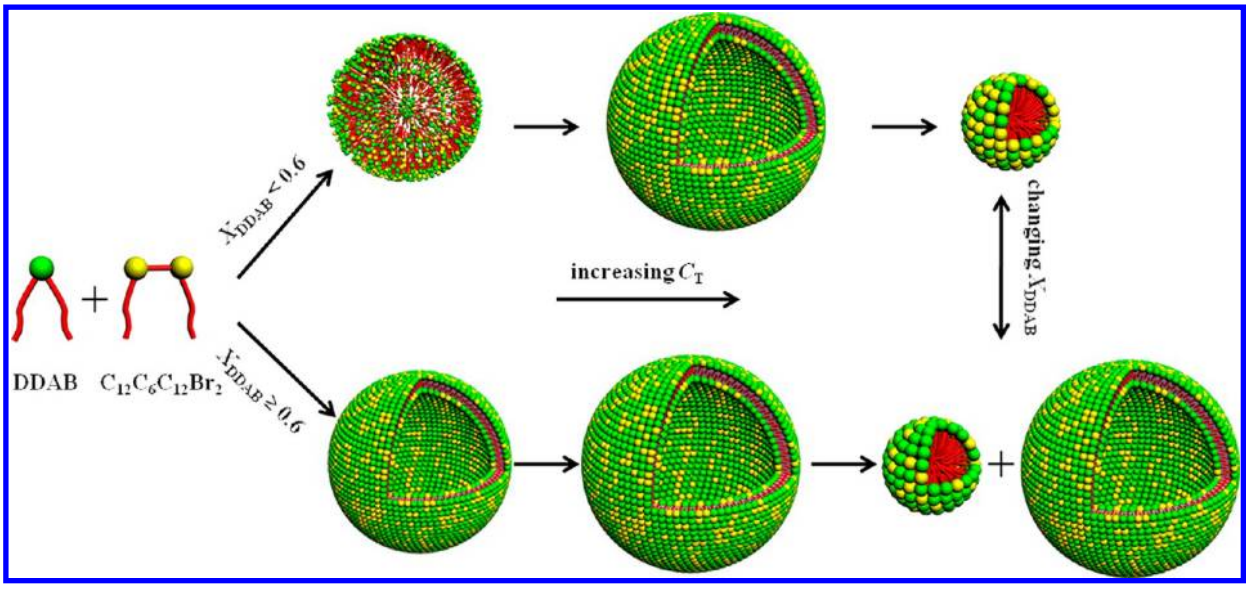

Figure 9. Possible models of aggregate transitions in the DDAB/$C_{12}C_6C_{12}Br_2$ mixtures.

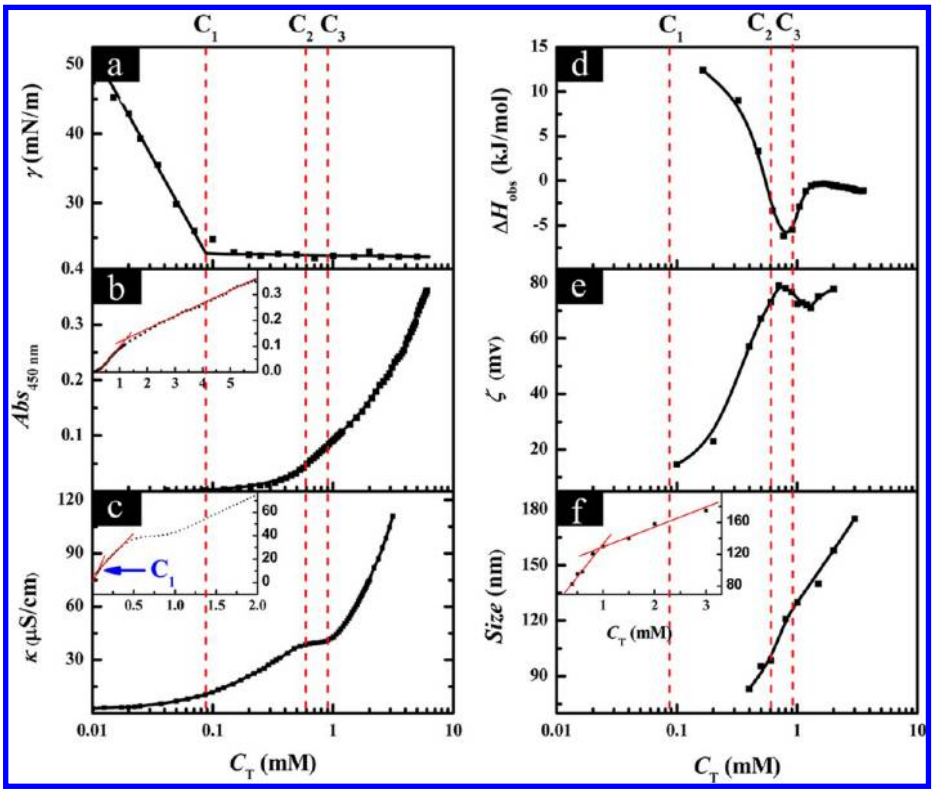

Figure 10. Variations of (a) surface tension, (b) turbidity, (c) electrical conductivity, (d) observed enthalpy change (ΔH_{obs}), (e) ζ potential, and (f) aggregate size of the DDAB/$C_{12}C_6C_{12}Br_2$ mixtures plotted against C_T on a logarithmic scale at 25.0 °C (X_{DDAB} = 0.8).

This implies that all of the protons move into a more hydrophobic environment in the transition from vesicles to micelles and that the headgroups experience more significant variations in this transition. These results help us to understand the variations in the molecular packing in the aggregate transitions.

By combining all of the measurements in the mixtures of DDAB and $C_{12}C_6C_{12}Br_2$ at X_{DDAB} = 0.3, the possible models of the aggregate transitions are illustrated in the top line of Figure 9. The DDAB/$C_{12}C_6C_{12}Br_2$ mixtures start to self-assemble at C_1. In the region of $C_1 \approx C_2$, spherical aggregates of ~20 nm are the main aggregates, where the hydrophobic microdomain may be not as neat as in the vesicles and the bilayer fragments may be cross-linked. The turbidity and ζ potential increase, but the aggregation degree of ionization and surface tension decrease in the transition. In the region of $C_2 \approx C_3$, spherical aggregates transfer to large vesicles. The surface tension stops decreasing. Simultaneously, the aggregation degree of ionization further decreases while the turbidity and ζ potential keep increasing. Above C_3, the vesicles start to transfer to small spherical micelles. The aggregation degree of ionization continues to decrease, and the turbidity and ζ potential of

dx.doi.org/10.1021/la301762g | *Langmuir* 2012, 28, 12005−12014

the aggregates also begin to decrease. However, the surface tension starts to increase. This means that at this stage the surfactants prefer to form micelles in the bulk solution rather than assemble at the air/water interface.

Aggregation Behavior at X_{DDAB} = 0.8. Figure 10 displays curves of (a) surface tension, (b) turbidity, (c) electrical conductivity, (d) observed enthalpy change, (e) ζ potential, and (f) aggregate size of the DDAB/$C_{12}C_6C_{12}Br_2$ mixtures plotted against C_T at X_{DDAB} = 0.8. Figure 11 shows the ITC

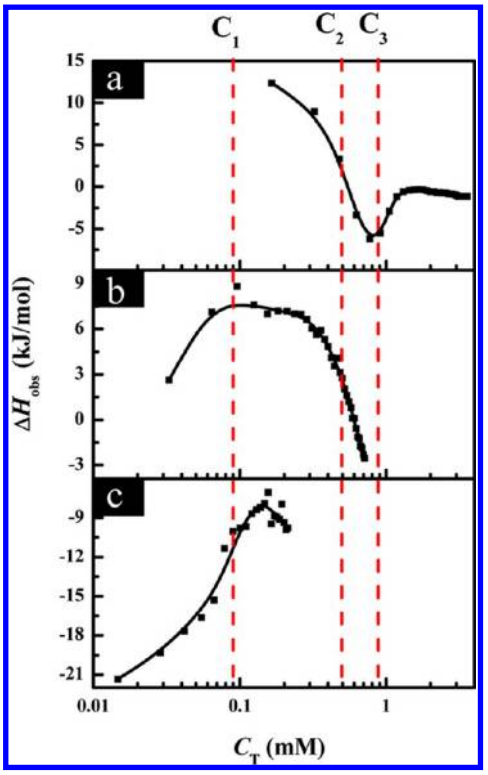

Figure 11. Observed enthalpy ΔH_{obs} vs C_T on a logarithmic scale for the titration of (a) 10.00, (b) 2.00, and (c) 0.60 mM DDAB/$C_{12}C_6C_{12}Br_2$ mixtures into water at 25.00 °C (X_{DDAB} = 0.8).

curves of ΔH_{obs} against C_T via titrating the DDAB/$C_{12}C_6C_{12}Br_2$ mixtures of different initial concentrations (10.0, 2.0, and 0.6 mM) into water. By combining all of the results from different techniques, the curves against C_T are clearly divided into four variation regions, which are below C_1 (C_T < 0.08 mM), between C_1 and C_2 (0.08−0.49 mM), between C_2 and C_3 (0.49−0.89 mM), and beyond C_3 (C_T > 0.89 mM). The morphologies of the mixed DDAB/$C_{12}C_6C_{12}Br_2$ aggregates in the four regions were characterized by cryo-TEM. Below C_1, no aggregates were observed. The representative images of the aggregates in the other three regions (C_1 to C_2, C_2 to C_3, and beyond C_3) are exhibited in Figure 12 and the Supporting Information (Figure S5).

As shown in Figures 10 and 11, all of the curves present a critical point at C_1 except the curves of the ζ potential and size. The surface tension declines sharply to C_1 and then maintains its value close to that of the pure DDAB solution. Different from that at X_{DDAB} = 0.3, the surface tension curve shows only one critical concentration. Herein, beyond C_1, the turbidity and ζ potential increase gradually as C_T increases. Meanwhile, the aggregation degree of ionization from the conductivity curve becomes smaller and the ΔH_{obs} decreases in the ITC curve. All

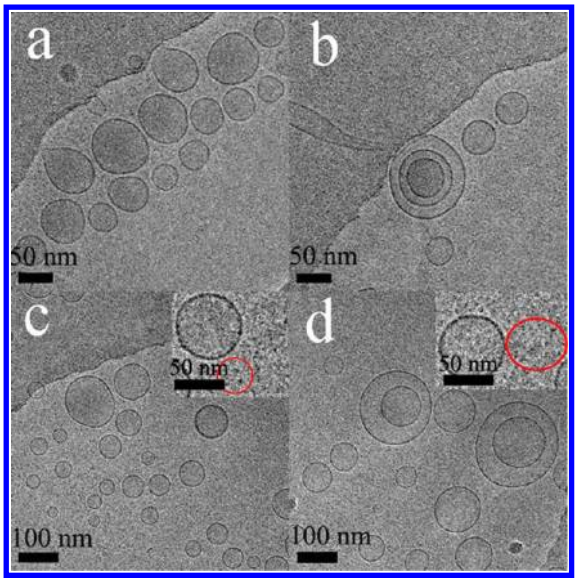

Figure 12. Cryo-TEM images of the DDAB/$C_{12}C_6C_{12}Br_2$ aggregates at C_T values of (a) 0.30, (b) 0.60, (c) 1.00, and (d) 4.00 mM. The insets of c and d are enlarged images of small spherical micelles (X_{DDAB} = 0.8).

of these results indicate that the aggregates begin to form beyond C_1. The cryo-TEM image (Figure 12a) shows that in the region of C_1 to C_2 the main aggregates are vesicles of 50−80 nm.

In the region of C_2 to C_3, the size of the aggregates continues to increase while the ζ potential goes over a maximum but without a significant change in value. In particular, an obvious platform appears in the conductivity curve. Normally, the electrical conductivity of the systems containing ionic surfactant aggregates mainly depends on free ions. Here, with the increase in C_T, the unchanged conductivity indicates that the free ions do not increase correspondingly. Therefore, the newly added surfactants are mainly absorbed by the vesicles, and the vesicles grow between C_2 and C_3 as proven by the increases in turbidity (Figure 10b) and size (Figure 10d). However, the vesicles in the cryo-TEM image (Figure 12b) are not obvious larger than those at C_1 to C_2. The possible reason is that the hole of the carbon membrane on the TEM grids cannot bear aggregates that are too large.

Beyond C_3, the cryo-TEM images (Figure 12c,d) show that vesicles and micelles coexist in the mixed solution. Obvious changes can be observed in all of the curves except in the surface tension measurement. The conductivity increases rapidly after the platform, the ΔH_{obs} value begins to increase, and the ζ potential begins to decrease slightly. All of these variations are in accord with the vesicle-to-micelle transition. Because the transition is not finished in this period, the turbidity and the aggregate size keep increasing but at a slower rate. When the vesicles and micelles reach a balance, the ΔH_{obs} value becomes zero. Then, a further increase in C_T leads to only an increase in the number of mixed aggregates.

To obtain a further explanation of the aggregate transitions, more investigations were carried out as follows. The systematic ITC measurement was carried out by titrating the DDAB/$C_{12}C_6C_{12}Br_2$ solutions at different initial concentrations into water (Figure 11). Because the initial concentrations of 10.0 and 1.0 mM are higher than those of C_3 and the initial concentration of 0.6 mM is within C_2 to C_3, the DDAB/

dx.doi.org/10.1021/la301762g | Langmuir 2012, 28, 12005−12014

$C_{12}C_6C_{12}Br_2$ mixtures exist as a micelle/vesicle mixture in the initial solutions of 10.0 and 2.0 mM but as larger vesicles in the initial solution of 0.6 mM. From Figure 11a,b, the ΔH_{obs} values when the final concentration is within C_1 to C_2 indicate that the process of the added micelle/vesicle mixture changing to vesicles is endothermic. Conversely, as the final concentration increases from C_1 to C_2 and C_3, both the vesicle formation and growth are exothermic and are promoted by the enhanced hydrophobic interaction and the resultant decreased degree of ionization of the vesicles. As seen from Figure 11c, when the vesicle solution is titrated into water and the final concentration is below C_1, the exothermic ΔH_{obs} indicates that the transition from vesicles to monomers must be accompanied by the strong hydration and ionization of the surfactants.

In brief, by combining the measurements in the DDAB/$C_{12}C_6C_{12}Br_2$ mixtures at X_{DDAB} = 0.8, the possible models of aggregate transitions at high X_{DDAB} are illustrated in the bottom line of Figure 9. With the increase in C_T, the DDAB/$C_{12}C_6C_{12}Br_2$ mixtures start to self-assemble at C_1 and form vesicles between C_1 and C_2, followed by their growth between C_2 and C_3. Then the vesicles begin to transfer to small spherical micelles at C_3, and finally a dynamic equilibrium between spherical micelles and vesicles is achieved above C_3.

Comparison of Aggregate Transitions at High and Low X_{DDAB}. As is well known, $C_{12}C_6C_{12}Br_2$ molecules self-assemble into spherical micelles and DDAB molecules begin to form vesicles at considerably low concentration.[28−30] Herein, in the DDAB/$C_{12}C_6C_{12}Br_2$ mixtures, the aggregate transitions have been realized through varying C_T and X_{DDAB}.

At lower C_T, DDAB and $C_{12}C_6C_{12}Br_2$ molecules exist as monomers in aqueous solution because the hydrophobic interaction between the alkyl chains is not strong enough to construct aggregates. With the increase in C_T, the hydrophobic interaction increases and hydrophobic chains begin to pack tightly, leading to the formation of vesicles at high X_{DDAB} ($\geq$0.6). Instead, at low X_{DDAB} (<0.6), the loose spherical aggregates are generated, where the hydrophobic interaction is still not strong enough to form a large, neat hydrophobic microdomain because of the low DDAB concentration. With further increasing C_T, the absolute DDAB concentration increases and the hydrophobic interaction increases. Even at low X_{DDAB}, the hydrophobic interaction of the DDAB/$C_{12}C_6C_{12}Br_2$ mixture is strong enough to assemble into vesicles. According to Rubingh's theory,[37,38] the mole fraction of DDAB in the DDAB/$C_{12}C_6C_{12}Br_2$ aggregates (α_{DDAB}) has been estimated as shown in Supporting Information (Table S1), which may help us to illustrate the formation of vesicles even at low X_{DDAB}. The calculated results indicate that even if X_{DDAB} is low there are more DDAB molecules in the mixed aggregates (i.e., the DDAB molecules are the main contributor). Because the DDAB molecules prefer to form vesicles, the DDAB/$C_{12}C_6C_{12}Br_2$ mixtures can form vesicles at low X_{DDAB} but require enough C_T.

At high C_T (higher than C_3), the vesicles transfer to small spherical micelles whenever X_{DDAB} is low or high. However, the origin may be different. At low X_{DDAB}, $C_{12}C_6C_{12}Br_2$ is the main component, so the aggregation ability of $C_{12}C_6C_{12}Br_2$ is the leading factor in the aggregate formation of the mixtures. The strong electrostatic repulsion of the $C_{12}C_6C_{12}Br_2$ headgroups results in the formation of micelles. Nevertheless, at high X_{DDAB}, the formation of micelles is due to the increase in the absolute concentration of $C_{12}C_6C_{12}Br_2$ at high C_T.

CONCLUSIONS

In this work, the elaborate regulation of aggregate transitions in the DDAB/$C_{12}C_6C_{12}Br_2$ mixtures has been realized through gradually changing the total surfactant concentration C_T and the surfactant mole fraction. When C_T was constant, a spontaneous vesicle-to-micelle transition was found with decreasing X_{DDAB} at high C_T. At a given X_{DDAB}, various aggregates were obtained and their transitions were realized through changing C_T. At X_{DDAB} < 0.6, the gradually increasing C_T resulted in the formation of small loose spherical aggregates and large spherical vesicles and finally the transition from the vesicles into small micelles. However, at $X_{DDAB} \geq 0.6$ the increase in C_T led to the formation and growth of vesicles, the vesicle/micelle transition, and the final vesicle/micelle coexistence. The aggregate structures greatly influence the surface tension, turbidity, electrical conductivity, zeta potential, and intermolecular interactions of the DDAB/$C_{12}C_6C_{12}Br_2$ mixtures. The gradual variations of the hydrophobic interaction, electrostatic repulsion, and related degree of ionization and hydration of the surfactants should be responsible for the complicated aggregation behaviors. This work provides a successful example by applying two very similar surfactants to conveniently achieve different structural aggregates and finely adjust the properties of the aggregates, such as the size, charge properties, and surface activity. The results may help us to understand the intermolecular interaction in bicationic mixed surfactants further and to guide the design and control of self-assembled structures of mixed surfactants so as to gain the desired characteristics in applications.

ASSOCIATED CONTENT

Supporting Information

Determinations of critical concentrations from electrical conductivity curves. Additional cryo-TEM images. Observed enthalpy curves. ^{1}H NMR spectra of the DDAB, $C_{12}C_6C_{12}Br_2$, and DDAB/$C_{12}C_6C_{12}Br_2$ mixtures. This material is available free of charge via the Internet at http://pubs.acs.org.

AUTHOR INFORMATION

Corresponding Author

*E-mail: yilinwang@iccas.ac.cn.

Notes

The authors declare no competing financial interest.

ACKNOWLEDGMENTS

This work was supported by the Chinese Academy of Sciences and the National Natural Science Foundation of China (grants 21025313, 21021003, 20973181, and KJCX1-YW-21-02). We appreciate the State Key Laboratory of Polymer Physics and Chemistry for providing the DLS equipment.

REFERENCES

(1) Allen, T. M.; Cullis, P. R. Drug Delivery Systems: Entering the Mainstream. *Science* **2004**, *303*, 1818.

(2) Tanev, P. T.; Pinnavaia, T. J. Biomimetic Templating of Porous Lamellar Silicas by Vesicular Surfactant Assemblies. *Science* **1996**, *271*, 1267.

(3) Rai, P. R.; Saraph, A.; Ashton, R.; Poon, V.; Mogridge, J.; Kane, R. S. Raftlike Polyvalent Inhibitors of the Anthrax Toxin: Modulating Inhibitory Potency by Formation of Lipid Microdomains. *Angew. Chem., Int. Ed.* **2007**, *46*, 2207.

(4) Jiang, L. X.; Wang, K.; Deng, M. L.; Wang, Y. L.; Huang, J. B. Bile Salt-Induced Vesicle-to-Micelle Transition in Catanionic Surfactant

Systems: Steric and Electrostatic Interactions. *Langmuir* **2008**, *24*, 4600.
(5) Kaler, E. W.; Murthy, A. K.; Rodriguez, B. E.; Zasadzinski, J. A. N. Spontaneous Vesicle Formation in Aqueous Mixtures of Single-Tailed Surfactants. *Science* **1989**, *245*, 1371.
(6) Kaler, E. W.; Herrington, K. L.; Murthy, A. K.; Zasadzinski, J. A. N. Phase Behavior and Structures of Mixtures of Anionic and Cationic Surfactants. *J. Phys. Chem.* **1992**, *96*, 6698.
(7) Schubert, B. A.; Kaler, E. W.; Wagner, N. J. The Microstructure and Rheology of Mixed Cationic/Anionic Wormlike Micelles. *Langmuir* **2003**, *19*, 4079.
(8) Raghavan, S. R.; Fritz, G.; Kaler, E. W. Wormlike Micelles Formed by Synergistic Self-Assembly in Mixtures of Anionic and Cationic Surfactants. *Langmuir* **2002**, *18*, 3797.
(9) Lu, T.; Han, F.; Li, Z. C.; Huang, J. B.; Fu, H. L. Transitions of Organized Assemblies in Mixed Systems of Cationic Bolaamphiphile and Anionic Conventional Surfactants. *Langmuir* **2006**, *22*, 2045.
(10) Yan, Y.; Xiong, W.; Li, X. X.; Lu, T.; Huang, J. B.; Li, Z. C.; Fu, H. L. Molecular Packing Parameter in Bolaamphiphile Solutions: Adjustment of Aggregate Morphology by Modifying the Solution Conditions. *J. Phys. Chem. B* **2007**, *111*, 2225.
(11) Jiang, L. X.; Wang, K.; Deng, M. L.; Wang, Y. L.; Huang, J. B. Bile Salt-Induced Vesicle-to-Micelle Transition in Catanionic Surfactant Systems: Steric and Electrostatic Interactions. *Langmuir* **2008**, *24*, 4600.
(12) Davies, T. S.; Ketner, A. M.; Raghavan, S. R. Self-Assembly of Surfactant Vesicles That Transform into Viscoelastic Wormlike Micelles upon Heating. *J. Am. Chem. Soc.* **2006**, *128*, 6669.
(13) Huang, X.; Cao, M. W.; Wang, J. B.; Wang, Y. L. Controllable Organization of a Carboxylic Acid Type Gemini Surfactant at Different pH Values by Adding Copper(II) Ion. *J. Phys. Chem. B* **2006**, *110*, 19479.
(14) Lichtenberg, D. Characterization of the Solubilization of Lipid Bilayers by Surfactants. *Biochim. Biophys. Acta* **1985**, *821*, 470.
(15) Vinson, P. K.; Talmon, Y.; Walter, A. Vesicle-Micelle Transition of Phosphatidylcholine and Octyl Glucoside Elucidated by Cryo-Transmission Electron Microscopy. *Biophys. J.* **1989**, *56*, 669.
(16) Walter, A.; Vinson, P. K.; Kaplun, A.; Talmon, Y. Intermediate Structures in the Cholate-Phosphatidylcholine Vesicle-Micelle Transition. *Biophys. J.* **1991**, *60*, 1315.
(17) Edwards, K.; Almgren, M. Solubilization of Lecithin Vesicles by C12E8: Structural Transitions and Temperature Effects. *J. Colloid Interface Sci.* **1991**, *147*, 1.
(18) Edwards, K.; Almgren, M.; Bellare, J.; Brown, W. Effects of Triton X-100 on Sonicated Lecithin Vesicles. *Langmuir* **1989**, *5*, 473.
(19) Edwards, K.; Gustafsson, J.; Almgren, M.; Karlsson, G. Solubilization of Lecithin Vesicles by a Cationic Surfactant: Intermediate Structures in the Vesicle-Micelle Transition Observed by Cryo-Transmission Electron Microscopy. *J. Colloid Interface Sci.* **1993**, *161*, 299.
(20) Silvander, M.; Karlsson, G.; Edwards, K. Vesicle Solubilization by Alkyl Sulfate Surfactants: A Cryo-TEM Study of the Vesicle to Micelle Transition. *J. Colloid Interface Sci.* **1996**, *179*, 104.
(21) Israelachvili, J.; Mitchell, D.; Ninham, B. Theory of Self-Assembly of Hydrocarbon Amphiphiles into Micelles and Bilayers. *J. Chem. Soc., Farady Trans.* **1976**, *172*, 1525.
(22) Zana, R. Ionization of Cationic Micelles: Effect of the Detergent Structure. *J. Colloid Interface Sci.* **1980**, *78*, 330.
(23) Menger, F. M.; Keiper, J. S. Gemini Surfactants. *Angew. Chem., Int. Ed.* **2000**, *39*, 1906.
(24) Zana, R. Gemini (Dimeric) Surfactants. *Curr. Opin. J. Colloid Interface Sci.* **1996**, *1*, 566.
(25) Zana, R.; Talmon, Y. Dependence of Aggregate Morphology on Structure of Dimeric Surfactants. *Nature* **1993**, *362*, 624.
(26) Danino, D.; Talmon, Y.; Zana, R. Vesicle-to-Micelle Transformation in Systems Containing Dimeric Surfactants. *J. Colloid Interface Sci.* **1997**, *185*, 84.
(27) Anne, B. G.; Zana, R.; Talmon, Y. Microstructures in Aqueous Solutions of Mixed Dimeric Surfactants: Vesicle Transformation into Networks of Thread-Like Micelles. *J. Phys. Chem. B* **2000**, *104*, 12192.
(28) Caria, A.; Regev, O.; Khan, A. Surfactant - Polymer Interactions: Phase Diagram and Fusion of Vesicle in the Didodecyldimethylammonium Bromide-Poly(ethylene oxide)-Water System. *J. Colloid Interface Sci.* **1998**, *200*, 19.
(29) Treiner, C.; Makayssi, A. Structural Micellar Transition for Dilute Solutions of Long Chain Binary Cationic Surfactant Systems: A Conductance Investigation. *Langmuir* **1992**, *8*, 794.
(30) Regev, O.; Khan, A. Vesicle-Lamellar Transition Events in DDAB-Water Solution. *Prog. Colloid Polym. Sci.* **1994**, *97*, 298.
(31) Zana, R.; Benrraou, M.; Rueff, R. Alkanediyl-α,ω-bis-(dimethylalkylammonium bromide) Surfactants. 1. Effect of the Spacer Chain Length on the Critical Micelle Concentration and Micelle Ionization Degree. *Langmuir* **1991**, *7*, 1072.
(32) Wang, C.; Huang, J.; Tang, S.; Zhu, B. Special Surface and Aggregation Behavior of a Novel Amino Acid Amphiphile. *Langmuir* **2001**, *17*, 6389.
(33) Han, Y. C.; Wang, Y. L. Aggregation Behavior of Gemini Surfactants and Their Interaction with Macromolecules in Aqueous Solution. *Phys. Chem. Chem. Phys.* **2011**, *13*, 1939.
(34) Aratono, M.; Onimaru, N.; Yoshikai, Y.; Shigehisa, M.; Koga, I. Spontaneous Vesicle Formation of Single Chain and Double Chain Cationic Surfactant Mixtures. *J. Phys. Chem. B* **2007**, *111*, 107.
(35) Mukerjee, P.; Mysels, K. J.; Dulin, C. Dilute Solutions of Amphipathic Ions. I. Conductivity of Strong Salts and Dimerization. *J. Phys. Chem.* **1958**, *62*, 1390.
(36) Clunie, J. S.; Goodman, J. F.; Symons, P. C. Electrical Conductance of Sodium n-Alkyl Sulphonates in Aqueous Solution. *Trans. Faraday Soc.* **1967**, *63*, 754.
(37) Holland, P. M.; Rubingh, D. N. Nonideal Multicomponent Mixed Micelle Model. *J. Phys. Chem.* **1983**, *87*, 1984.
(38) Rubingh, D. N. Mixed Micelle Solutions. In *Solution Chemistry of Surfactants*; Mittal, K. L., Ed.; Plenum Press: New York, 1979; Vol. *1*, p 337.